Welding in the World (2025) 69:3809–3821
https://doi.org/10.1007/s40194-025-02150-y

RESEARCH PAPER

Effect of post-weld heat treatment on the mechanical performance of 2.25Cr-1Mo-0.2 V welded joints assessed via Small Punch Testing

M. M. Llera[1] · G. Álvarez[1] · A. Zafra[2] · C. Rodríguez[1]

Received: 11 March 2025 / Accepted: 17 August 2025 / Published online: 5 September 2025

Abstract
The influence of a post-weld heat treatment (PWHT) on the microstructure and mechanical behaviour of a 2.25Cr1Mo0.25 V weld was investigated. The study focused on three distinct regions: the base metal, the heat-affected zone (HAZ), and the weld metal. Due to the limitations in conducting standard mechanical tests on all the weld regions, particularly the HAZ, Small Punch Tests (SPT) were performed across all regions, while standard mechanical tests were conducted only when sufficient material was available. Microstructural characterisation involved microstructure identification, hardness profiling, X-ray diffraction measurements, and fractographic examination. The results demonstrate that the SPT method effectively characterises the mechanical behaviour of all weld regions. Furthermore, PWHT significantly enhances microstructural homogeneity and improves the mechanical performance of both the HAZ and weld metal. The treatment leads to relaxation of residual stresses and microstructural refinement, thereby increasing the resistance of welded components to mechanical failure.

Keywords Welded joint · Post-welding heat treatment (PWHT) · Heat-affected zone (HAZ) · Small Punch Test (SPT)

1 Introduction

In conventional structural calculations, materials are often assumed to be homogeneous throughout the component. However, most real structures include welded joints, making this assumption unrealistic. When a structure incorporates welds, calculations are typically based on the weld geometry and follow safety parameters outlined in the Eurocode standards [1]. Nonetheless, the integrity of the component can only be ensured if the welding procedure has been correctly executed. Even slight deviations during welding may result in joints that perform significantly worse than the base metal, introducing a potential weakness in the structure.

CrMoV steels are extensively used in high-temperature and corrosive environments due to their excellent strength and corrosion resistance. Consequently, these steels are widely employed in critical pressure equipment subjected to severe service conditions, including oil and gas storage vessels, thermal and nuclear power components, and steam turbine cylinder blocks [2, 3]. Such critical components must satisfy strict reliability and safety requirements. Since welded joints typically represent the weakest link in these structures, ensuring their integrity is essential for overall structural safety.

Welding involves complex, highly localised thermal cycles [4–7], which induce sharp microstructural gradients from the base metal (BM) through the heat-affected zone (HAZ), and into the weld metal (WM). Among these regions, the coarse-grained HAZ (CGHAZ) is particularly susceptible to brittle failure due to increased hardness and reduced toughness. However, accurately characterising the mechanical response of individual zones, especially the HAZ, remains challenging due to its limited size and difficulty obtaining standard test specimens.

Authors such as Nagaraju et al. [8] have studied different welding processes in steels and reported that mechanical properties such as yield stress and ultimate tensile strength typically decrease progressively from the WM to the BM,

Recommended for publication by Commission IX - Behaviour of Metals Subjected to Welding

✉ M. M. Llera
lleramarcos@uniovi.es

[1] SIMUMECAMAT Research GroupWest Departmental BuildingPolytechnic School of EngineeringPrincipality of Asturias, Universidad de Oviedo, 7.1.10, 33203 Gijón, Spain

[2] Mechanics of Materials Lab Department of Engineering Science, University of Oxford, Oxford OX1 3PJ, UK

whereas ductility and toughness exhibit the opposite trend. Nonetheless, their analysis excluded the HAZ due to difficulties in sample extraction, resulting in a notable gap in experimental data, particularly for the CGHAZ, despite its critical role in joint integrity.

Post-weld heat treatments (PWHTs) are frequently applied to welded structures to enhance toughness and ductility and reduce residual stresses, significantly modifying the mechanical behaviour of weld zones. Several studies [9–12] have investigated the effects of various PWHTs on CrMoV steels using standard tensile and fracture specimens taken from the WM and BM regions. Their findings consistently show that increasing PWHT temperatures reduce strength but enhance elongation and fracture toughness. However, the small size of the HAZ (and especially the CGHAZ) generally prohibits extracting standard mechanical test samples, leaving the mechanical response of this critical region largely unexplored.

Many existing studies have evaluated the mechanical behaviour of welded joints using specimens encompassing entire weld regions rather than individual constituents. Although practical, this approach fails to isolate the specific contributions from each microstructural zone and may be significantly influenced by local defects or residual stresses, masking the intrinsic behaviour of critical regions such as the CGHAZ [13]. Additionally, obtaining standard specimens from weld zones often demands partial or complete shutdown of equipment, causing increased costs and downtime. This is particularly problematic for components already in service. To overcome these challenges, researchers have focused on miniaturising test samples [14–16], allowing highly localised mechanical characterisation using minimal amounts of material. The primary goal of these studies is to obtain results comparable to conventional tests while significantly reducing specimen dimensions. Small specimens can even be extracted from in-service structures without compromising structural integrity, enabling continuous assessment of welded joints and monitoring their mechanical properties over time—particularly advantageous in aggressive service environments.

This miniaturisation approach is especially beneficial for welded joints, where spatial resolution is crucial. Due to the minimal dimensions of the HAZ [17, 18] obtaining standard test specimens from this region alone is nearly impossible. Some studies have attempted to replicate the CGHAZ and other HAZ sub-zones by applying controlled thermal cycles intended to approximate welding conditions [5, 6, 19–22]. However, this method is costly, complex, and typically produces approximations rather than fully representative microstructures, limiting its accuracy [19].

Alternatively, other authors [15, 23] have pursued direct sampling of small homogeneous micro-volumes from welded joints, using non-standard specimens to assess the true mechanical response of each individual zone. For instance, Xue et al. [18] tested QP980 steel welds with non-standard miniature tensile specimens focusing on small fusion zones, revealing a higher susceptibility of the CGHAZ to brittle fracture. Similarly, Sánchez et al. [24] successfully miniaturised fracture toughness specimens for in-service components, demonstrating the effectiveness of small-scale mechanical testing. Nevertheless, challenges persist, particularly regarding the complexity and cost of fabricating these miniature specimens.

The present work aims to bridge this gap by employing the Small Punch Test (SPT), one of the most widely used miniature testing techniques [14, 16, 25–28]. Originally developed for applications in the nuclear industry, SPT has since been adopted broadly for characterising metallic materials. This technique uses simple, disc-shaped specimens (typically 10×10 mm with a thickness of 0.5 mm), effectively capturing the tensile behaviour of steels with varying microstructures and mechanical properties [15]. The simplicity and small size of SPT specimens facilitate easy machining, further enhancing the practicality of this method for localised assessment of welded joints.

The main objective of this study is to systematically evaluate the effect of PWHT on the tensile and fracture properties of the different zones within a CrMoV steel welded joint, with particular attention to the critical CGHAZ. SPT samples were extracted from each weld region (BM, WM, HAZ) before and after PWHT. The results from SPT tests performed on WM and BM samples were compared with conventional tensile and fracture tests to establish correlations between miniature and standard methods. Additionally, the study examines the influence of PWHT on microstructure and hardness, complemented by X-ray diffraction (XRD) analysis to quantify microstructural distortions, providing deeper insight into the mechanical responses observed.

2 Materials and experimental procedures

2.1 Materials

This study investigates the effect of PWHT on a 2.25Cr1Mo0.25 V welded joint. A butt joint was produced between two SA 542 Grade-D-Class4 steel plates, each measuring 108 mm in thickness, 275 mm in width, and 750 mm in length. The welding process employed submerged arc welding (SAW) with DC current and a heat input of 2.2 kJ/mm (29–32 V, 425–550 A, welding speed 45–55 cm/min), using Thyssen Union S1 CrMo2V electrodes as filler material. Preheating temperatures ranged between 205 and 250 °C. Further welding information is available in the work by G. Álvarez et al. [15]. After welding, the joint was subjected

to a dehydrogenation treatment at 350 °C for 4 h and subsequently divided into two parts. One part was analysed in the as-welded condition (AW), while the other was subjected to a PWHT at 705 °C for 10 h, followed by air cooling at room temperature. Therefore, the experimental characterisation described below compares these two conditions: as-welded (AW) and post-weld heat treated (PWHT).

2.2 Microstructural analysis

To characterise the microstructure of each welded coupon, samples were ground progressively up to #1200-grit SiC paper and polished to a 1 µm diamond finish. Microstructures from the different weld zones were revealed using a 5% Nital etching solution and examined under a Nikon V12 optical microscope. Hardness across each weld zone was measured using Vickers indentation tests (HV1) performed with a Buehler Serie 2100 hardness tester. Additionally, X-ray diffraction (XRD) analyses were carried out to assess differences in the crystalline structures of the weld zones, using a Stresstech Xstress 3000 G3 diffractometer with CrKα radiation, a vanadium filter, and operating conditions of 30 kV and 6.7 mA. Variations in crystallographic lattice distortions were assessed by calculating the full width at half maximum (FWHM) values from the ferrite (α − iron) {211} diffraction peak at $2\theta = 156.1°$, using an exposure time of 20 s [29, 30].

2.3 Mechanical characterisation

2.3.1 Tensile and fracture toughness tests

The different zones of both welded joints were characterised using standard tensile and fracture toughness tests to allow direct comparison with results obtained by SPT. As standard mechanical tests require relatively larger volumes of material, they were only conducted in weld zones where sufficient material was available—specifically, the BM and WM—as shown schematically in Fig. 1.

Tensile tests were executed according to the UNE-EN-ISO 6892 standard [31], using round specimens with a diameter of 10 mm and a gauge length of 70 mm. Tests were carried out at room temperature using a MTS universal testing machine equipped with a 100 kN load cell and an Epsilon axial extensometer. The applied strain test rate was $2.2 \times 10^{-4}\ s^{-1}$, with three specimens tested per region (BM and WM) in each weld condition.

Fracture toughness tests were performed according to ASTM E1820 [32], employing single-edge notched bend (SE(B)) specimens measuring $225 \times 50 \times 25$ mm (length (L) × width (W) × thickness (B)). A minimum of three specimens per weld region in each condition were tested. Specimens were first fatigue pre-cracked to achieve an initial crack length-to-width ratio (a/W) of 0.5, followed by side-grooving to achieve a thickness reduction of 0.2B mm. Fracture toughness testing was carried out using the same MTS machine as for tensile tests, equipped with an MTS crack opening displacement (COD) extensometer to measure crack growth via the compliance method. A displacement rate of 0.5 mm/min was used. The single-specimen unloading compliance method was employed to obtain the J-Δa resistance curves, where the increase in crack length (Δa) and corresponding fracture toughness (J) values were determined at each unload/reload step. The critical fracture toughness parameter (J_Q) was identified as the value of J at a 0.2 mm crack extension, determined by the intersection of the power-law regression fitted to the J-Δa curve and the 0.2 mm offset blunting line [32].

After fracture toughness testing, specimens were fatigue-loaded until complete fracture occurred, enabling subsequent fractographic analysis. Fracture surfaces were examined using a JEOL-JSM5600 scanning electron microscope (SEM) to investigate the failure micromechanisms in each testing region.

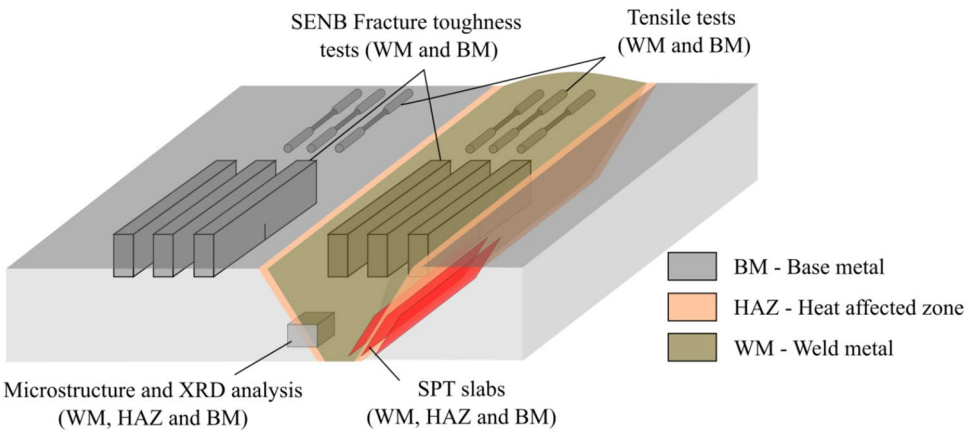

Fig. 1 Scheme of the welded coupon showing the extraction orientation of specimens from the base metal (BM), weld metal (WM), and heat-affected zone (HAZ) in both the as-welded (AW) and post-weld heat-treated (PWHT) conditions

2.3.2 Small Punch Tests

Small Punch Tests were conducted using a standardised testing setup (Fig. 2*a*) complying with the UNE EN 10371 standard [26]. The SPT device comprises a lower supporting die with a central hole (4 mm in diameter and 0.2 mm chamfer radius) and a semi-spherical punch head (2.5 mm diameter). The detailed description of the SPT device is provided elsewhere [14]. Tests were performed using an electromechanical Instron machine equipped with a 5 kN load cell. Punch displacement relative to the upper die was measured using a COD extensometer.

After clearly identifying each weld zone—weld metal (WM), base metal (BM), and coarse grain from the heat-affected zone (CG-HAZ) (Fig. 1)—0.5 ± 0.1 mm thick sheets were extracted from these regions by electrical discharge machining (EDM). From these sheets, square SPT specimens measuring 10 × 10 mm were prepared. Prior to testing, the specimens were ground and polished to achieve a final thickness of 0.5 ± 0.01 mm and cleaned thoroughly with acetone. Specimen thickness was precisely verified using a micrometre with a resolution of 0.5 µm.

SPTs were conducted at a constant punch displacement rate of 0.2 mm/min, testing a minimum of three specimens per weld zone and treatment condition. After testing, load–displacement curves were analysed to extract characteristic values: yield load (P_y), maximum load (P_m), and displacement at maximum load (d_m) (Fig. 2*b*). Based on previous successful correlations [14], the yield load (P_y) in this work was specifically defined at the intersection of the load–displacement curve with the offset line drawn at *t*/10 (10% of specimen thickness) from the initial elastic slope ($P_{y\_t/10}$). The corresponding values for yield stress (σ_{ys}) and ultimate tensile strength (σ_{ut}) were then calculated using Eqs. (1) and (2), proposed by García et al. [14].

$$\sigma_{ys} = \alpha \cdot \frac{P_{y_{-t/10}}}{t^2}\,[\mathrm{MPa}] \tag{1}$$

$$\sigma_{ut} = \beta \cdot \frac{P_m}{d_m t}\,[\mathrm{MPa}] \tag{2}$$

where $P_{y\_t/10}$ is the yield load determined by the t/10 offset method, P_m and d_m are the load and displacement at the maximum load point, respectively, and $\alpha = 0.346$ and $\beta = 0.277$ are empirical constants obtained from prior calibrations [14].

After testing, specimens were sectioned through the fracture zone to examine their cross-section and measure the final thickness (t_f). The equivalent biaxial strain, (ε_{qf}) was then calculated using Eq. (3), and the material's fracture toughness was estimated using Eq. (4), previously proposed by García et al. [14]. This expression is valid provided the material exhibits sufficient ductility ($\varepsilon_{qf} > 0.78$).

$$\varepsilon_{qf} = \ln\left(\frac{t}{t_f}\right) \tag{3}$$

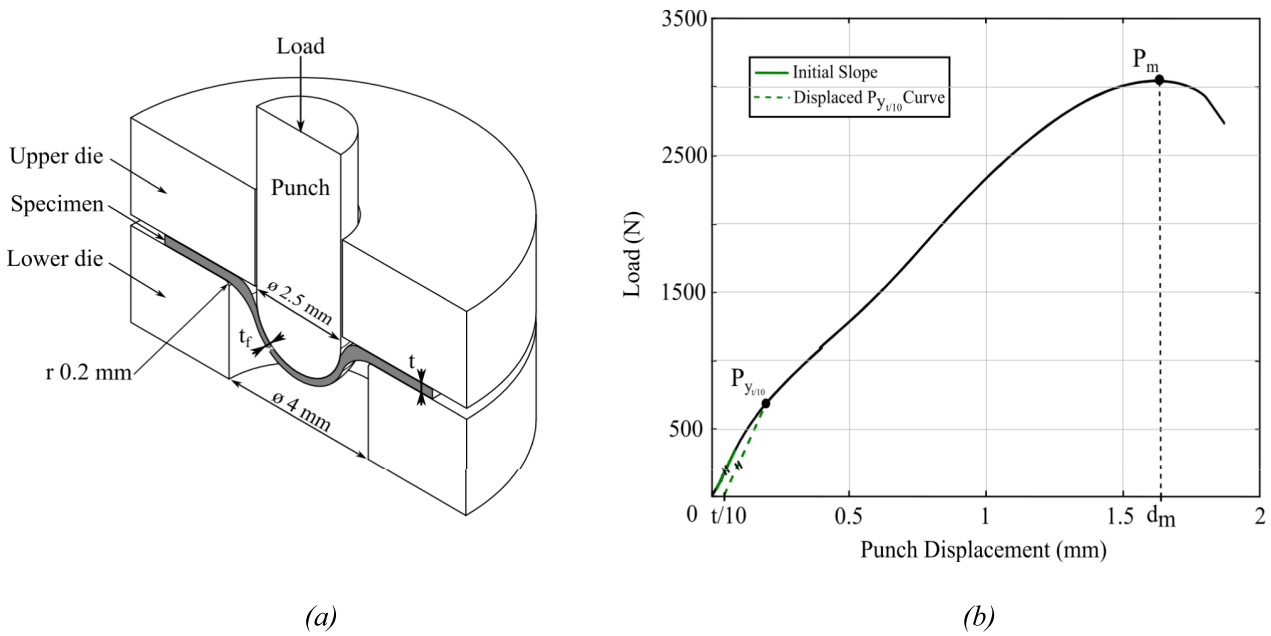

Fig. 2 ***a*** Small Punch Test setup used in the experiments. ***b*** Representative load–displacement SPT curve with the key values of load and dispacement used for mechanical property estimation.

$$J_Q = 1695\varepsilon_{qf} - 1320\left[\frac{kJ}{m^2}\right] \quad (4)$$

Additionally, fractographic analysis of all specimens was conducted using SEM to identify general fracture characteristics and evaluate the dominant micromechanisms of failure.

3 Results

3.1 Microstructure and hardness

Figure 3 presents the macro and microstructures of the welded joints in the as-welded (AW, Fig. 3a) and post-weld heat-treated (PWHT, Fig. 3b) conditions. The three characteristic zones (BM, HAZ, and WM) along with HAZ subzones (coarse grain zone, CGHAZ, fine grain zone, FGHAZ and intercritical zone, ICHAZ) are clearly identifiable. In the as-welded condition (Fig. 3a), all zones exhibit similar microstructures consisting of a mixture of bainite and martensite, differing primarily in grain geometry and size [33]. The base metal grain size of approximately 80 µm increases due to welding thermal cycles, reaching approximately 150 µm in the CGHAZ. From this coarsened grain structure, epitaxial growth occurs into the weld metal, forming columnar grains aligned along the solidification direction. After PWHT (Fig. 3b), the microstructure remains fundamentally similar, but a slight decomposition of martensitic and bainitic structures is observed [34, 35].

Hardness profiles measured across the different weld zones before and after PWHT are shown in Fig. 4a. The original BM hardness of approximately 228 HV1 (black triangles) increases significantly due to the welding thermal cycle, reaching a peak value of around 405 HV1 in the AW-CGHAZ (blue triangles), with a slight reduction to 381 HV1 in the AW-WM (red triangles). The softening effect of PWHT (circles in Fig. 4a) is evident in all weld zones but is particularly pronounced in the WM (222 HV1, red circles) and HAZ (247 HV1, blue circles), where hardness values decrease by more than 40%.

The FWHM parameter obtained from XRD analysis for the ferritic {211} diffraction peak ($2\theta = 156.1°$)is shown in Fig. 4b, illustrating the effect of thermal cycles induced by welding. Compared to the BM (black line), the WM (red line) and particularly the CGHAZ (blue line) exhibit broader and flatter diffraction peaks. This peak broadening is directly related to increased lattice distortion due to residual stresses and higher dislocation densities within these hardened zones. Following PWHT (dashed lines), a clear reduction in FWHM values is observed across all weld zones, confirming relaxation of residual stresses and decreased micro-strain. The narrowing of diffraction peaks after PWHT indicates reduced defect density and internal stresses. Additionally, peak positions after PWHT shift towards values closer to the unaltered base metal, further validating the stress-relief effect of the PWHT.

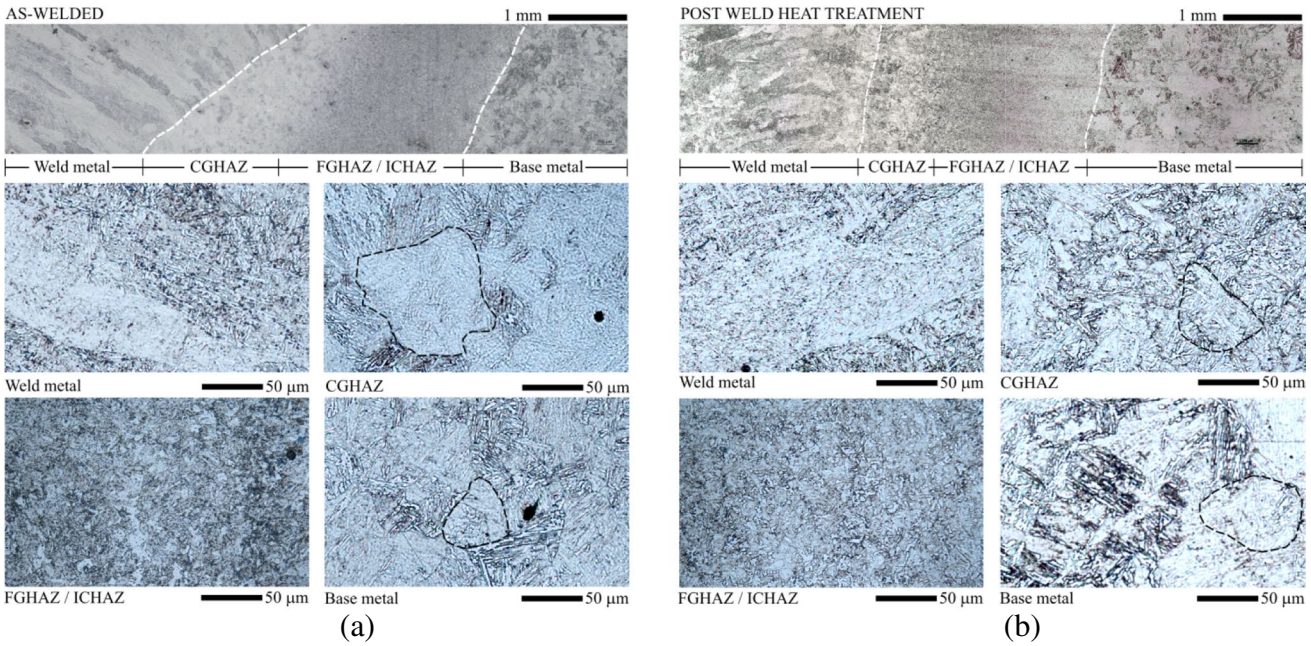

Fig. 3 Optical micrograph showing the different zones of the welded joints: **a** as-welded, AW; **b** after post-weld heat treatment, PWHT

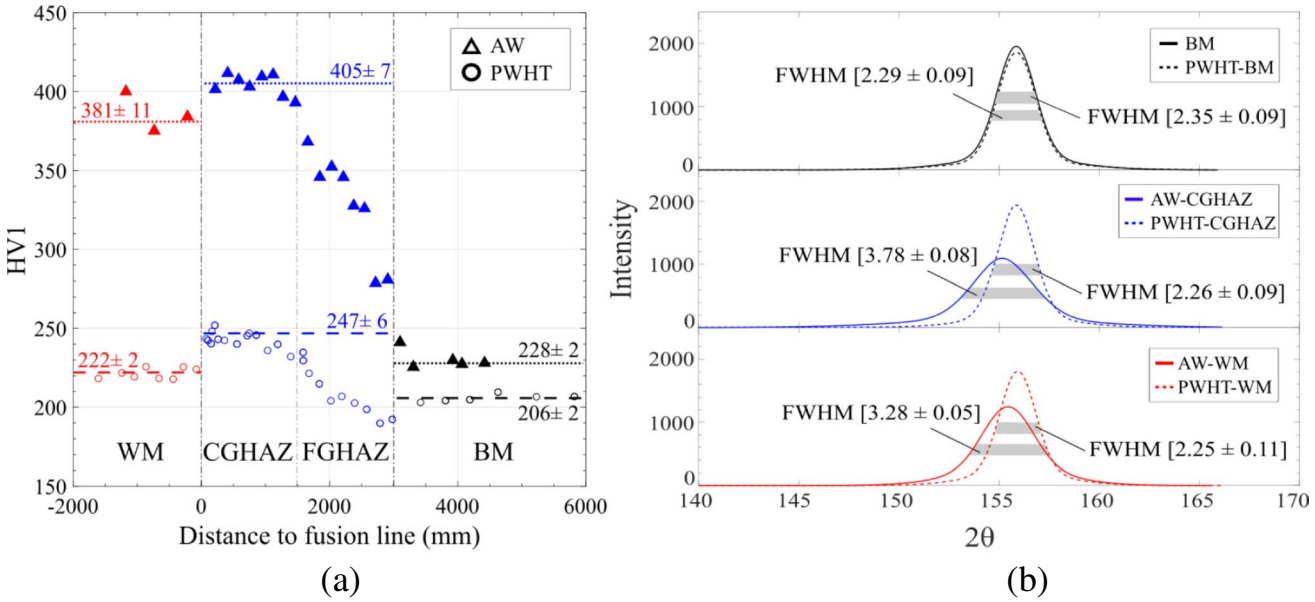

Fig. 4 **a** Hardness profiles across the welded joint in AW and PWHT conditions. **b** XRD measurements of the ferrite {211} diffraction peak in different weld zones.

Table 1 Tensile and fracture toughness properties (mean ± standard deviation) of the different zones of the welds, obtained using standard testing methods

Material	σ_{ys}[MPa]	σ_{ut} [MPa]	J_Q [kJ/m^2]
BM	597 ± 3.2	710 ± 2.3	750 ± 4.5
AW-WM	1019 ± 2.1	1120 ± 1.0	22 ± 8.1
PWHT-BM	550 ± 1.7	695 ± 7.2	649 ± 2.3
PWHT-WM	533 ± 5.6	631 ± 5.1	579 ± 7.6

3.2 Tensile and fracture toughness properties from standard test

Table 1 summarises the tensile and fracture toughness properties of the BM and WM in both the as-welded (AW) and post-weld heat-treated (PWHT) conditions. It is important to note that the mechanical properties of the heat-affected zone (HAZ) could not be obtained through standard testing methods due to the limited size of this region, which does not meet the dimensional requirements for conventional specimens.

As shown in Fig. 5a, the tensile curve for the as-welded weld metal (AW-WM) lies significantly above that of the base metal (BM). In agreement with the hardness results, the yield strength (σ_{ys}) and ultimate tensile strength (σ_{ut}) of the AW-WM are nearly twice those of the BM. Following PWHT, the tensile properties of the PWHT-BM remain largely unchanged. However, the mechanical strength of the PWHT-WM is substantially reduced, approaching values similar to those of the PWHT-BM. This suggests a significant softening and homogenisation effect of the PWHT on the weld metal.

Figure 5b displays the J-Δa resistance curves for the BM and WM before and after PWHT. In the as-welded condition, the WM exhibits extremely low fracture toughness, characterised by brittle behaviour. In fact, the critical fracture toughness value (J_Q) for the AW-WM had to be derived from K_{IC}, indicating limited plasticity prior to fracture. In contrast, the BM shows high fracture toughness, consistent with ductile fracture mechanisms. After PWHT, and in contrast to the strength and hardness results, the fracture toughness of the WM increases markedly, reaching values comparable to those of the BM. This improvement confirms a significant microstructural homogenisation across the welded joint induced by the heat treatment.

Figure 6 further illustrates the contrasting fracture micromechanisms between BM and WM in the as-welded condition. The BM shows extensive microvoid coalescence (Fig. 6a), indicative of fully ductile failure. By contrast, the WM surface is characterised by flat facets typical of cleavage fracture, which correlates with its low toughness and brittle behaviour. After PWHT, both the BM and WM exhibit ductile fracture features dominated by microvoid coalescence, similar to those observed in the as-welded BM (Fig. 6a), confirming the enhanced toughness and ductility of the weld metal following the heat treatment.

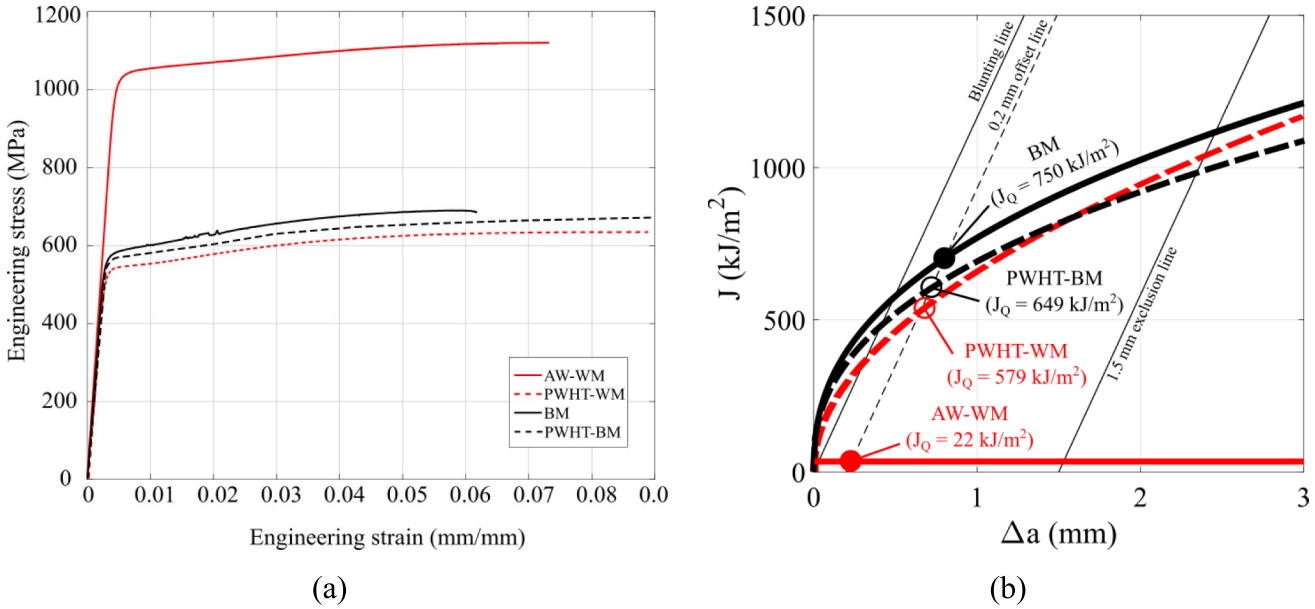

Fig. 5 Mechanical test results from standard specimens: **a** engineering stress–strain curves from tensile tests; **b** J-Δa curves from fracture toughness tests

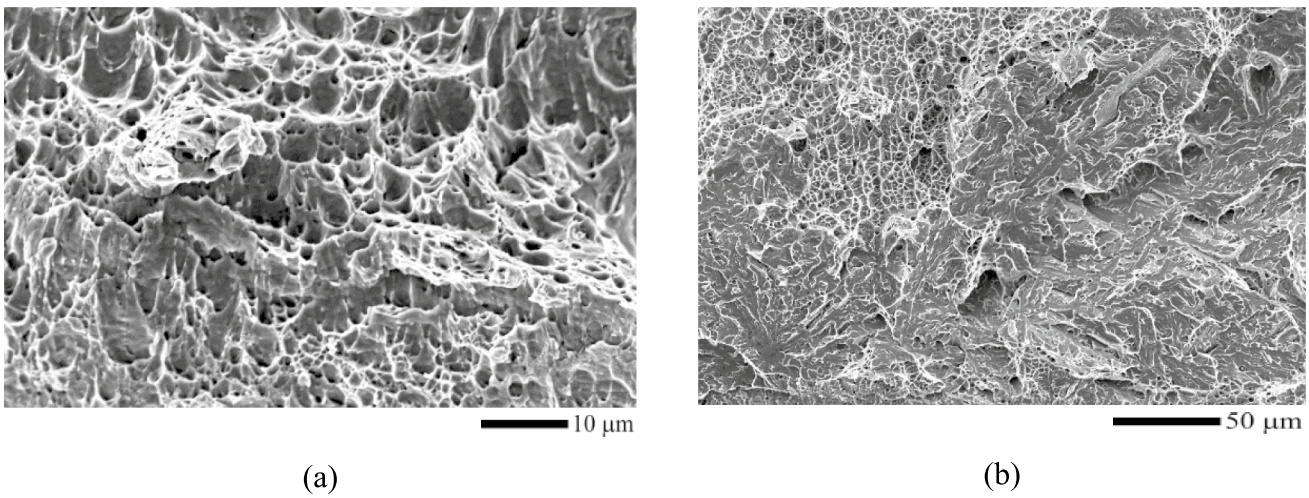

Fig. 6 SEM images of fracture surfaces from standard fracture toughness tests. **a** Ductile fracture in BM; **b** brittle cleavage fracture in AW-WM

3.2.1 SPT properties

The small size of the HAZ prevents its characterisation using standard tensile and fracture toughness tests, which require relatively large volumes of material [31, 32]. This limitation is overcome by using the SPT, which enables the extraction and testing of miniature specimens from all regions of the welded joint, including the CGHAZ.

Figure 7a shows representative load-punch displacement curves for the three main weld zones in both the AW (solid lines) and PWHT (dashed lines) conditions. In the AW condition, the WM and CGHAZ exhibit higher maximum loads than the BM, reflecting their higher strength. After PWHT, however, the load–displacement curves of all weld zones (dashed lines) converge and align closely with that of the BM, indicating a homogenisation of mechanical behaviour throughout the weldment.

These trends are consistent with the fracture surface morphologies shown in Fig. 7b. Fracture surfaces of AW-CGHAZ and AW-WM specimens display prominent secondary radial cracks (indicated by white arrows), a hallmark of

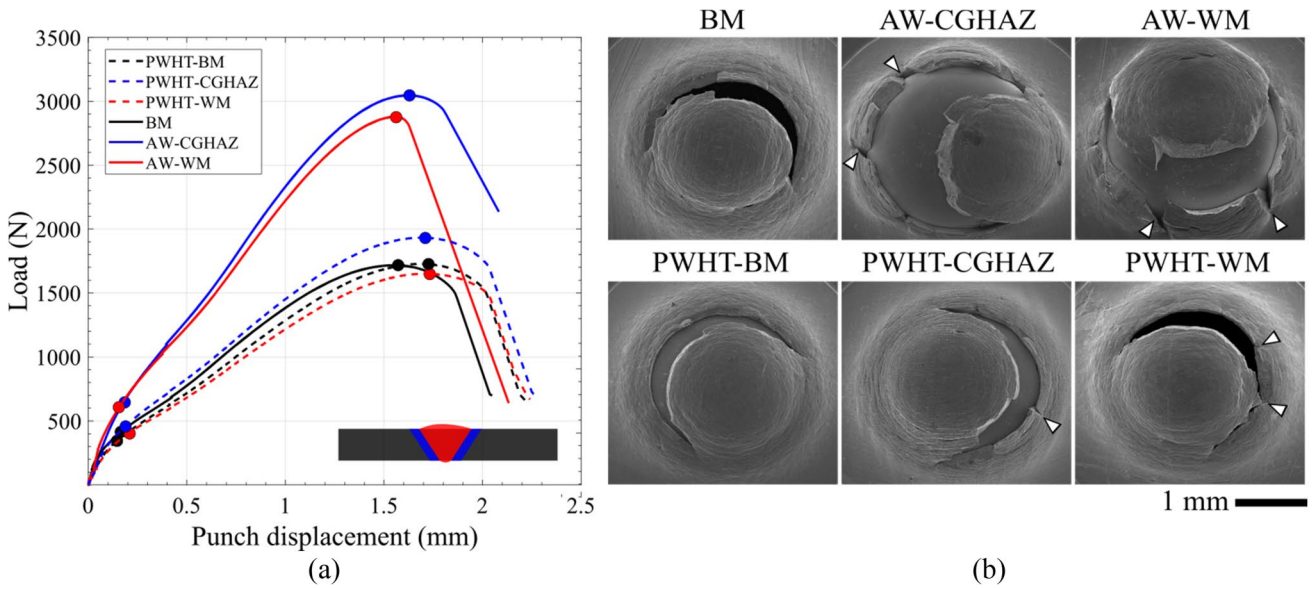

Fig. 7 SPT results for AW and PWHT welds; **a** representative load–displacement curves fused to extract tensile parameters; **b** fracture surfaces of SPT specimens showing failure morphology

Table 2 SPT parameters (mean ± standard deviation) obtained for the different weld zones in AW and PWHT conditions

Material		P_y/t^2 [MPa]	$P_m/(t \cdot d_m)$[MPa]	ε_{qf} [-]
AW	BM	1404 ± 257	2204 ± 46	1.23 ± 0.3
	CGHAZ	3301 ± 134	3755 ± 291	0.94 ± 0.2
	WM	2686 ± 401	3690 ± 333	0.77 ± 0.2
PWHT	BM	1418 ± 146	1993 ± 140	1.15 ± 0.1
	CGHAZ	1526 ± 323	2001 ± 264	1.12 ± 0.3
	WM	1651 ± 90	2159 ± 157	1.18 ± 0.2

brittle fracture. By contrast, the PWHT specimens from all the weld zones show fully ductile fracture surfaces, characterised by typical circumferential crack profiles with no observable radial or secondary cracking [36].

From the load–displacement curves, the load (P_y and P_m) and displacement (d_m) values were extracted and used to calculate the SPT parameters related with yield stress and ultimate tensile strength via Eqs. (1) and (2), respectively. The corresponding values obtained are presented in Table 2, along with the equivalent biaxial strain calculated using Eq. (3).

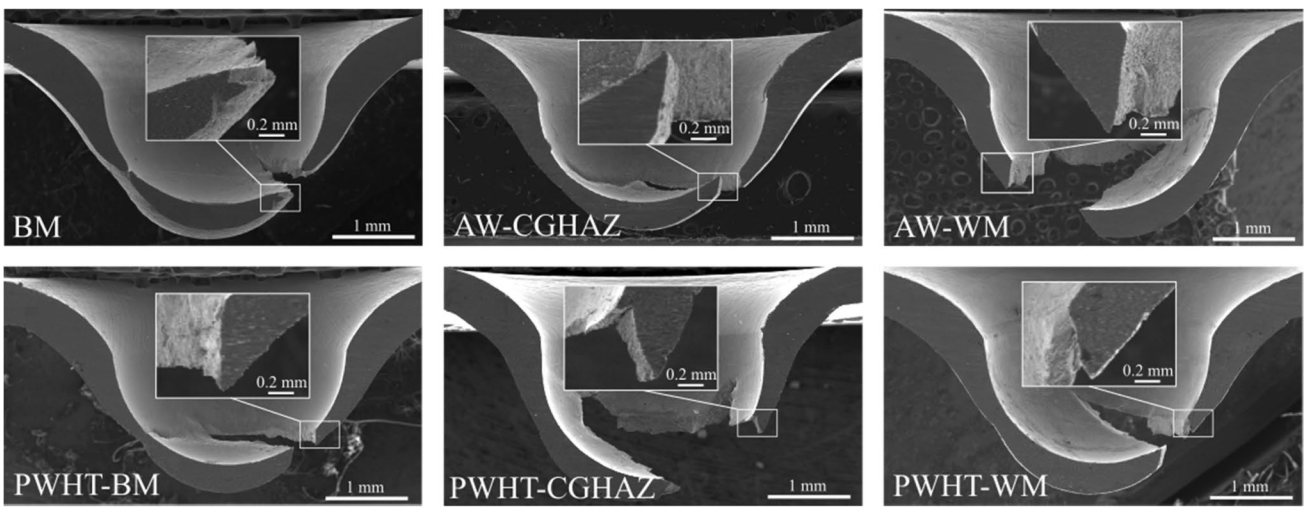

Fig. 8 Cross-section of SPT specimen in AW and PWHT conditions, used for measuring biaxial deformation and final specimen thickness for fracture toughness estimation

To determine the equivalent biaxial strain, cross-sections of the fractured specimens were examined. Figure 8 shows regions where the final thickness was measured. A smaller reduction in thickness is observed in the AW-CGHAZ and AW-WM specimens, confirming their lower ductility compared to the PWHT and BM conditions.

Figure 9 presents SEM images of the fracture surfaces from SPT specimens extracted from the WM in both conditions. In the AW condition (Fig. 9a), the surface features a combination of cleavage facets and microvoids, indicating incomplete ductile behaviour. After PWHT (Fig. 9b), the surface shows a more homogeneous distribution of microvoids, confirming improved plastic deformation capacity.

Table 3 summarises the tensile and fracture toughness properties estimated from the SPT data using the empirical correlations defined in Eqs. (1)–(4). The values obtained for the BM and WM in both conditions are slightly conservative compared to those obtained from standard mechanical testing, thus providing a safe approximation. Given the good agreement between SPT-based and standard measurements in these zones, it is reasonable to consider the mechanical property estimates for the CGHAZ derived solely from SPT data as reliable. Therefore, the SPT offers a valid and effective means to characterise the tensile and fracture toughness behaviour of weld regions, such as the CGHAZ, that are inaccessible to conventional testing methods.

Table 3 Mechanical properties (mean ± standard deviation) estimated from SPT data using Eqs. (1), (2), and (4)

Material		σ_{ys} [MPa]	σ_{ut} [MPa]	J_Q [kJ/m^2]
AW	BM	486 ± 89	610 ± 13	773 ± 53
	CGHAZ	950 ± 46	1040 ± 81	280 ± 120
	WM	929 ± 138	1022 ± 92	< 40
PWHT	BM	490 ± 51	552 ± 39	637 ± 61
	CGHAZ	571 ± 31	598 ± 44	683 ± 33
	WM	528 ± 112	554 ± 73	580 ± 172

4 Discussion

This study evaluates the influence of post-weld heat treatment (PWHT) on the mechanical behaviour of a CrMoV welded joint. One of the key effects of PWHT is the reduction of weld overmatching, as reported in previous studies [37]. The heat treatment promotes carbon diffusion out of metastable phases (such as martensite and bainite), leading to the precipitation of new carbides—primarily in the WM and CGHAZ—or the coarsening of existing ones, particularly in the BM [38]. As a result, the microstructure becomes more homogeneous and less distorted. Similar trends were observed by Qian Guo et al. [39] in CrMoV base and filler metals, where PWHT produced uniform microstructures characterised by columnar grains in the WM, tempered martensite in the HAZ, and tempered granular bainite, with microhardness values ranging from 200 to 300 HV. The homogenising effect of PWHT is clearly confirmed by the X-ray diffraction (XRD) analysis (Fig. 4b). After PWHT, the full width at half maximum (FWHM) of the diffraction peaks decreases across all regions of the weld, indicating reduced dislocation density and lattice distortion. In the as-welded (AW) condition, the diffraction peaks—particularly in the WM and CGHAZ—are broader and shifted to lower 2θ angles, reflecting significant internal stress and microstructural inhomogeneity. Following PWHT, the peaks become narrower and shift back towards higher angles, consistent with a stress-relieved and more

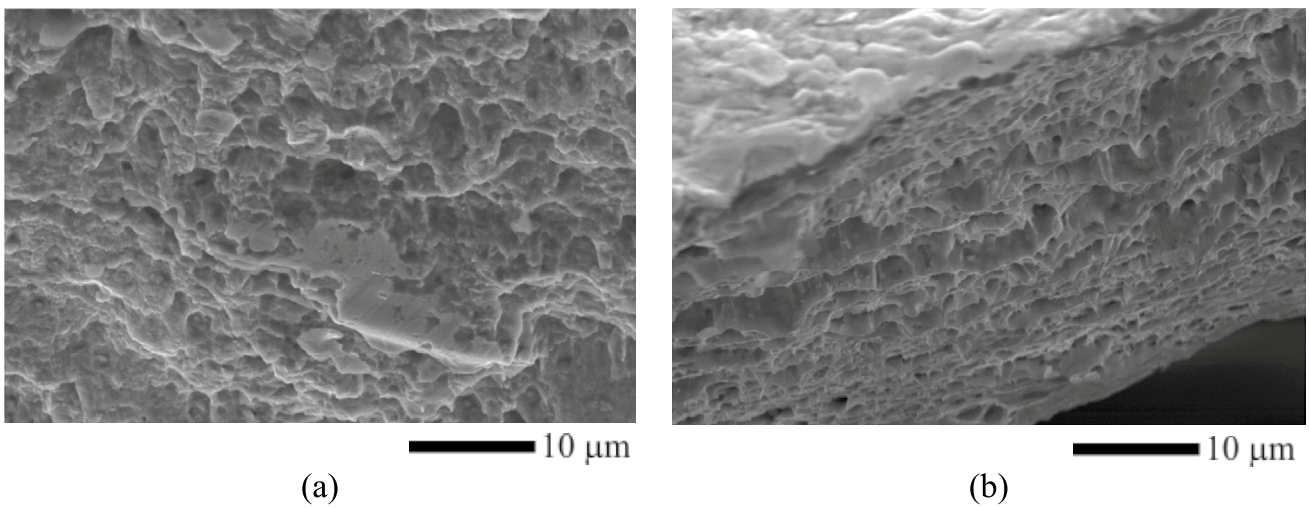

Fig. 9 SEM images of fracture micromechanism on SPT specimens from the weld metal: **a** AW-WM (×2500); **b** PWHT-WM (×2500)

uniform microstructure. These observations align with the mechanical results obtained via SPT and provide microstructural confirmation of the stress-relieving and homogenising effects of the heat treatment. The SPT results demonstrate strong agreement with the mechanical properties obtained from standard tensile and fracture toughness tests for both BM and WM (Table 1), validating the empirical correlations proposed by García et al. [14]. The good correlation allows the mechanical properties of the CGHAZ—unmeasurable by conventional tests due to geometric constraints—to be estimated with confidence. In the as-welded condition, the tensile properties of the CGHAZ derived from SPT closely match those of the WM, consistent with the similar hardness values observed in both regions (Fig. 4a). However, the fracture toughness of the CGHAZ is higher than that of the WM but still lower than the BM. This behaviour is consistent with findings by Rankumar et al. [9] and can be attributed to the more homogeneous microstructure of the CGHAZ compared to the WM. The WM typically exhibits large columnar grains and less uniform carbide dispersion, while the CGHAZ benefits from a more even distribution of carbides, which enhances fracture resistance. As supported by previous studies [40, 41], uniformly dispersed carbides can act as obstacles to dislocation motion and stress concentration, thereby improving fracture toughness.

Following PWHT, the more tempered and relaxed microstructures contribute to the mechanical homogenisation across all weld zones. Strength and hardness values in the PWHT condition become nearly equal across the BM, CGHAZ, and WM, with only slightly reduced values compared to the BM. The beneficial effect of PWHT is even more pronounced in terms of fracture toughness. All zones exhibit comparable toughness, approaching the values of the BM. This improvement is attributed to the precipitation of finely dispersed Cr–Mo carbides, which impede damage propagation and enhance crack resistance, particularly in the CGHAZ and WM [42]. In contrast, the PWHT has a minor, slightly detrimental effect on the fracture toughness of the BM. Since the BM already contains a well-distributed network of Cr–Mo carbides, the heat treatment primarily results in carbide coarsening [19], which slightly reduces fracture toughness. This coarsening may also account for the slight increase in lattice distortion observed in the PWHT-BM, as evidenced by the modest rise in FWHM in Fig. 4b. The local strain fields associated with carbide growth introduce subtle distortions detectable via XRD, although the overall impact remains limited due to the already tempered nature of the base metal.

The bar chart in Fig. 10 highlights the homogenisation effect of PWHT, showing that the mechanical

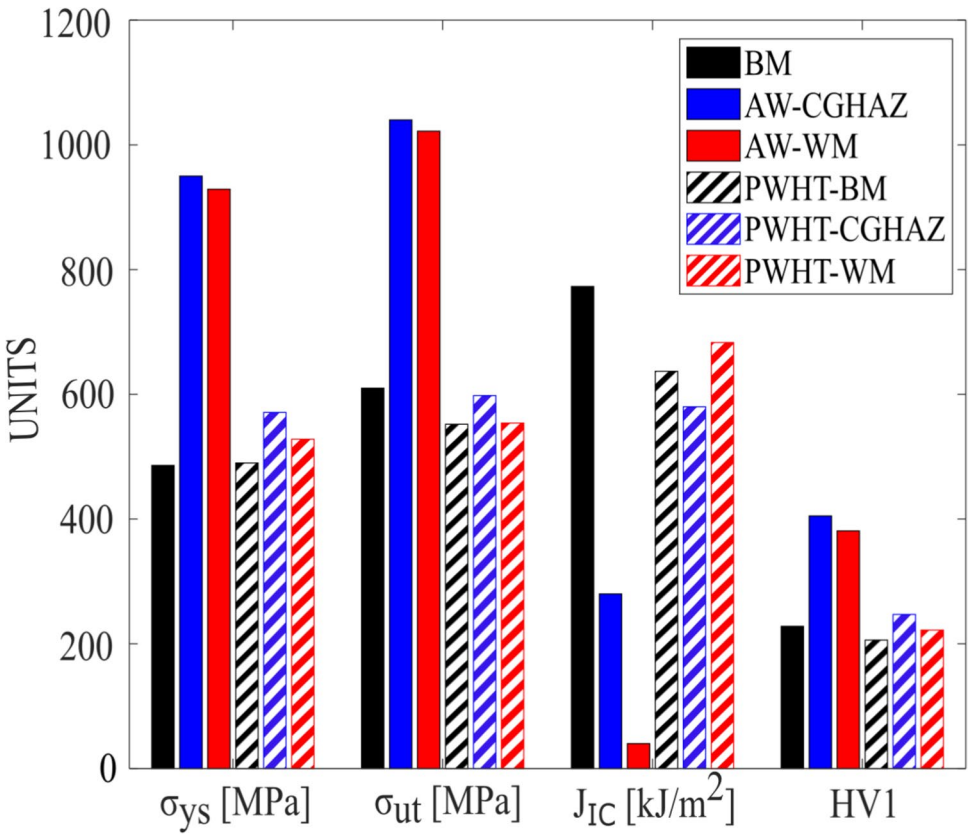

Fig. 10 Bar charts comparing the mechanical properties of BM, CGHAZ, and WM before and after PWHT, illustrating the homogenising effect of the heat treatment

properties of all zones in the treated condition (hatched bars) converge closely to those of the BM (solid black bar).

In conclusion, this work demonstrates the clear benefits of PWHT in enhancing the mechanical performance and uniformity of CrMoV welded joints. These insights would not have been possible without the use of the Small Punch Test, which enabled the characterisation of the CGHAZ—arguably the most critical and vulnerable region of the weld, and one that cannot be assessed using conventional mechanical tests.

5 Conclusions

In this work, the influence of post-weld heat treatment (PWHT) on the microstructure and mechanical behaviour of a 2.25Cr1Mo0.25 V welded joint has been evaluated using the Small Punch Test (SPT) technique. The main findings and technical contributions are summarised as follows:

- PWHT significantly reduces the mismatch in mechanical properties between the weld metal (WM), coarse-grained heat-affected zone (CGHAZ), and base metal (BM). After treatment, the strength, hardness, and fracture toughness values in all regions converge towards those of the base metal, indicating substantial homogenisation of the welded joint.
- X-ray diffraction (XRD) analysis supports the stress-relieving and homogenising effect of PWHT, showing reduced lattice distortion and dislocation density—particularly in the WM and CGHAZ—through narrower diffraction peaks and lower FWHM values after PWHT.
- The empirical correlations proposed by García et al. [6] for estimating tensile properties (σ_{YS}, σ_{ut}) and fracture toughness (J_{Ic}), from SPT data have been validated, with values closely matching those obtained from standard mechanical tests.
- The SPT technique enabled the mechanical characterisation of the CGHAZ, a zone typically inaccessible to conventional testing due to its small size and microstructural complexity.
- This study demonstrates that, when combined with complementary microstructural techniques such as hardness mapping and XRD, the SPT provides an effective, minimally invasive approach for assessing the mechanical integrity of complex welded joints, particularly in service-aged or safety–critical components where traditional testing methods are not feasible.

Authors' contributions M.M.Llera: writing—original draft, writing—review and editing, software, methodology, investigation, formal analysis, and data curation. M.M.Llera: writing—original draft, writing—review and editing, software, methodology, investigation, formal analysis, and data curation. G. Álvarez: writing—review and editing, software, methodology, formal analysis, investigation, data curation, conceptualization, and visualisation. A. Zafra: writing—review and editing, software, methodology, formal analysis, investigation, data curation, conceptualization, and visualisation. C. Rodríguez: conceptualization, funding acquisition, methodology, writing—review and editing, validation, visualisation, resources, project administration, and investigation.

Funding Open Access funding provided thanks to the CRUE-CSIC agreement with Springer Nature. Thanks to the Ministry of Economy and Competitiveness for the funding received in the framework of project PID2021-124768OB-C22 and to the Principality of Asturias for AYUD-2021–50985 research projects, to the Spanish Ministry of Science, Innovation and Universities, and to the Universidad de Oviedo for the financial support received for Guillermo Álvarez's Margarita Salas postdoctoral grant MU-21-UP2021-03. Thanks also to the Scientific-Technical Services of the Universidad de Oviedo for the use of the SEM JEOL-JSM5600 scanning electron microscope.

Data availability The data supporting the findings of this study are available from the corresponding author upon reasonable request.

Declarations

Competing interests The authors declare no competing interests.

References

1. AENOR. UNE-EN 1993–1–8:2011. Eurocode 3: Steel Structure Project. Part 1–8: Joints. https://www.aenor.com/
2. ASME BPVC.II.C-2019 Boiler and pressure vessel code. International code. Section II. 2019. https://www.asme.org/
3. Hucinska J (2003) Advanced vanadium modified steels for high pressure hydrogen reactors. Adv Mater Sci 4:21–27. Available: https://www.pg.gda.pl/mech/kim/AMS/022003/ams022003004.pdf
4. Radaj D (n.d.) Heat effects of welding. Temperature field, residual stress, distortion. https://doi.org/10.1007/978-3-642-48640-1
5. Zhou P, Wang B, Wang L, Hu Y, Zhou L (2018) Effect of welding heat input on grain boundary evolution and toughness properties in CGHAZ of X90 pipeline steel. Mater Sci Eng A 722:112–121. https://doi.org/10.1016/j.msea.2018.03.029
6. Zhao W, Wang W, Chen S, Qu J (2011) Effect of simulated welding thermal cycle on microstructure and mechanical properties of

X90 pipeline steel. Mater Sci Eng A 528(24):7417–7422. https://doi.org/10.1016/j.msea.2011.06.046
7. Bhardwaj S, Ratnayake RMC (2020) Challenges due to welds fabricated at a close proximity on offshore structures, pipelines, and piping: state of the art. https://doi.org/10.1115/OMAE2020-18586
8. Nagaraju S, Vasantharaja P, Brahadees G, Vasudevan M, Mahadevan S (2017) Effect of welding processes on the microstructure, mechanical properties and residual stresses of plain 9Cr-1Mo steel weld joints. J Mater Eng Perform 26(12):5938–5953. https://doi.org/10.1007/s11665-017-3077-9
9. Ramkumar P, Gupta RK, Kumar VA, Muthupandi V (2021) Effect of pre- and post weld heat treatment on microstructure development and mechanical properties of 0.3%C-CrMoV (ESR) high-strength low-alloy steel. J Mater Eng Perform 30(10):7835–7850. https://doi.org/10.1007/s11665-021-05929-4
10. Çalık A, Dokuzlar O, Uçar N (2020) The effect of heat treatment on mechanical properties of 42crmo4 steel. J Achiev Mater Manuf Eng 98(1):5–10. https://doi.org/10.5604/01.3001.0014.0811
11. Kulkarni A, Dwivedi DK, Vasudevan M (2018) Study of mechanism, microstructure and mechanical properties of activated flux TIG welded P91 steel-P22 steel dissimilar metal joint. Mater Sci Eng A 731(March):309–323. https://doi.org/10.1016/j.msea.2018.06.054
12. Storesund J, Sandström R (1995) Influence of post weld heat treatment on impact toughness properties of 1Cr0.5Mo and 2.25Cr1Mo steels. Steel Res 66(3):117–123. https://doi.org/10.1002/srin.199501099
13. Li Q, Cheng G, Qin M, Wang Y, Zhang Z (2021) Research on carbide characteristics and their influence on the properties of welding joints for 2.25Cr1Mo0.25V steel. Materials (Basel) 14(4):1–21. https://doi.org/10.3390/ma14040891
14. García TE, Rodríguez C, Belzunce FJ, Suárez C (2014) Estimation of the mechanical properties of metallic materials by means of the small punch test. J Alloys Compd 582:708–717. https://doi.org/10.1016/j.jallcom.2013.08.009
15. Álvarez G, Zafra A, Rodríguez C, Belzunce FJ, Cuesta II (2020) SPT analysis of hydrogen embrittlement in CrMoV welds. Theor Appl Fract Mech. https://doi.org/10.1016/j.tafmec.2020.102813
16. Arunkumar S, Korean Institute of Metals and Materials (2020) Overview of small punch test. Metals Mater Int 26(6):719–738. https://doi.org/10.1007/s12540-019-00454-5
17. Hayhurst RJ, Mustata R, Hayhurst DR (2005) Creep constitutive equations for parent, type IV, R-HAZ, CG-HAZ and weld material in the range 565–640°C for Cr–Mo–V weldments. Int J Press Vessel Pip 82(2):137–144. https://doi.org/10.1016/j.ijpvp.2004.07.014
18. Xue J et al (2022) Local microstructure and mechanical characteristics of HAZ and tensile behavior of laser welded QP980 joints. Mater Sci Eng A 854:143862. https://doi.org/10.1016/j.msea.2022.143862
19. Zafra A, Álvarez G, Belzunce J, Alegre JM, Rodríguez C (2020) Fracture toughness of coarse-grain heat affected zone of quenched and tempered CrMo steels with internal hydrogen: fracture micromechanisms. Eng Fract Mech 241(October):2021. https://doi.org/10.1016/j.engfracmech.2020.107433
20. Arora KS, Pandu SR, Shajan N, Pathak P, Shome M (2018) Microstructure and impact toughness of reheated coarse grain heat affected zones of API X65 and API X80 linepipe steels. Int J Press Vessel Pip 163:36–44. https://doi.org/10.1016/j.ijpvp.2018.04.004
21. Zafra A, Belzunce J, Rodríguez C, Fernández-Pariente I (2020) Hydrogen embrittlement of the coarse grain heat affected zone of a quenched and tempered 42CrMo4 steel. Int J Hydrogen Energy 45(33):16890–16908. https://doi.org/10.1016/j.ijhydene.2020.04.097
22. Czeskleba D, Nietzke J, Rhode M, Kannengiesser T (2023) Investigation of stress relief crack susceptibility of CrMoV steels coarse grain HAZ via simulation of uniaxial stress conditions during PWHT. Weld World 67(9):2133–2141. https://doi.org/10.1007/s40194-023-01539-x
23. García TE, Rodríguez C, Belzunce FJ, Cuesta II (2016) Effect of hydrogen embrittlement on the tensile properties of CrMoV steels by means of the small punch test. Mater Sci Eng A 664:165–176. https://doi.org/10.1016/j.msea.2016.03.134
24. Sánchez M, Cicero S, Kirk M, Altstadt E, Server W, Yamamoto M (2023) Using mini-CT specimens for the fracture characterization of ferritic steels within the ductile to brittle transition range: a review. Metals. https://doi.org/10.3390/met13010176
25. Álvarez G, Rodríguez C, Belzunce FJ, García TE (2020) Use of notched small punch test specimens for the determination of fracture properties in structural steels. Theor Appl Fract Mech. https://doi.org/10.1016/j.tafmec.2019.102442
26. Norma UNE-EN 10371 (2022) Metallic materials. Miniature punching test method. [Online]. Available: www.une.org
27. Otero S, Álvarez G, Llera MM, Rodríguez C (2025) Fatigue characterisation of structural steel by means of the small punch test: development of a methodology. Theor Appl Fract Mech 135:104772. https://doi.org/10.1016/j.tafmec.2024.104772
28. Geng X, Peng J, Jiang L, Liu X, Tu Y, Xue Z (2023) Experimental study of mechanical properties and fracture modes in different regions of the nickel-based welding joint based on small punch test. Weld World 67(3):637–650. https://doi.org/10.1007/s40194-022-01451-w
29. Fitzpatrick ME, Fry AT, Holdway P, Kandil FA, Shackleton J, Suominen L (2005) Determination of residual stresses by X-ray diffraction. National Measurement Good Practice Guide No. 52. NPL. National Physical Laboratory. Available: http://eprintspublications.npl.co.uk/id/eprint/2391
30. Guo W, Francis JA, Li L, Vasileiou AN, Crowther D, Thompson A (2016) Residual stress distributions in laser and gas-metal-arc welded high-strength steel plates. Mater Sci Technol 32(14):1449–1461. https://doi.org/10.1080/02670836.2016.1175687
31. (2009) UNE-EN 10002–1. Metalic materials. Tensile test. Part 1. Test method at room temperature. https://www.une.org
32. ASTM E1820–09 (2009) Standard test method for measurement of fracture toughness. https://www.astm.org
33. Jiang Z, Wang P, Li D, Li Y (2017) The evolutions of microstructure and mechanical properties of 2.25Cr-1Mo-0.25V steel with different initial microstructures during tempering. Mater Sci Eng A 699(February):165–175. https://doi.org/10.1016/j.msea.2017.05.095
34. Schönmaier H, Fleißner-Rieger C, Krein R, Schmitz-Niederau M, Schnitzer R (2021) On the impact of post weld heat treatment on the microstructure and mechanical properties of creep resistant 2.25Cr–1Mo–0.25V weld metal. J Mater Sci 56(36):20208–20223. https://doi.org/10.1007/s10853-021-06618-2
35. Pereira PAS, Franco CSG, Guerra Filho JLM, Dos Santos DS (2015) Hydrogen effects on the microstructure of a 2.25Cr-1Mo-0.25V steel welded joint. Int J Hydrogen Energy 40(47):17136–17143. https://doi.org/10.1016/j.ijhydene.2015.07.095
36. García TE, Arroyo B, Rodríguez C, Belzunce FJ, Álvarez JA (2016) Small punch test methodologies for the analysis of the hydrogen embrittlement of structural steels. Theor Appl Fract Mech 86:89–100. https://doi.org/10.1016/j.tafmec.2016.09.005
37. Bastola A, Wang J, Shitamoto H, Mirzaee-Sisan A, Hamada M, Hisamune N (2017) Investigation on the strain capacity of girth welds of X80 seamless pipes with defects. Eng Fract Mech 180:348–365. https://doi.org/10.1016/j.engfracmech.2017.06.010

38. Schönmaier H, Musi M, Albu M, Krein R, Schnitzer R (2022) Effect of post weld heat treatment on the interplay of microstructure, precipitates and properties of creep-resistant 2.25Cr-1Mo-0.25V weld metal. Mater. Sci. Eng. A 850(January):143550. https://doi.org/10.1016/j.msea.2022.143550
39. Guo Q, Lu F, Liu X, Yang R, Cui H, Gao Y (2015) Correlation of microstructure and fracture toughness of advanced 9Cr/CrMoV dissimilarly welded joint. Mater Sci Eng A 638:240–250. https://doi.org/10.1016/j.msea.2015.04.011
40. Hong S et al (2013) Effects of intergranular carbide precipitation on delayed fracture behavior in three Twinning induced plasticity (TWIP) steels. Materials Science and Engineering: A 587:85–99. https://doi.org/10.1016/j.msea.2013.08.063
41. Wu Q, Lu F, Cui H, Ding Y, liu X, Gao Y (2014) Microstructure characteristics and temperature-dependent high cycle fatigue behavior of advanced 9% Cr/CrMoV dissimilarly welded joint. Mater Sci Eng A 615:98–106. https://doi.org/10.1016/j.msea.2014.07.067
42. Ding K, Wang P, Liu X, Li X, Zhao B, Gao Y (2018) Formation of lamellar carbides in alloy 617-HAZ and their role in the impact toughness of alloy 617/9%Cr dissimilar welded joint. J Mater Eng Perform 27(11):6027–6039. https://doi.org/10.1007/s11665-018-3668-0